

Lead/Scintillating Fiber Electromagnetic Calorimeter Prototype  
CLAS-NOTE 90-013

K. Beard, V. Burkert, R.A. Eisenstein, H.O. Funsten, M. Gai, K. Giovanetti,  
A.D. Hancock, K.J. Healey, D.W. Hertzog, D. Joyce, J.R. Kane, J. Lieb, W.F. Vulcan

October 25, 1990

# Lead/Scintillating Fiber Electromagnetic Calorimeter Prototype\*

K. Beard<sup>2</sup>, V. Burkert<sup>1</sup>, R.A. Eisenstein<sup>5</sup>, H.O. Funsten<sup>2</sup>, M. Gai<sup>6</sup>, K. Giovanetti<sup>3</sup>  
A.D. Hancock<sup>2</sup>, K.J. Healey<sup>3</sup>, D.W. Hertzog<sup>5</sup>, D. Joyce<sup>1</sup>, J.R. Kane<sup>2</sup>, J. Lieb<sup>4</sup>, W.F. Vulcan<sup>2</sup>

<sup>1</sup> CEBAF, Newport News, VA 23606, <sup>2</sup> College of William and Mary, Williamsburg, VA 23185,  
<sup>3</sup> James Madison University, Harrisonburg, VA 22807 <sup>4</sup> George Mason University, Fairfax, VA 22030  
<sup>5</sup> University of Illinois, Urbana, IL 61801 <sup>6</sup> Yale University, New Haven, CT 06511

## Abstract

Results of a test beam study at the AGS facility of the Brookhaven National Laboratory are presented for a large modular lead-scintillating fiber electromagnetic calorimeter. This prototype is one of two candidate sampling calorimeters for the CLAS detector in the Hall B experimental area of the CEBAF electron accelerator. The calorimeter is designed to provide good energy resolution, good position resolution, and excellent electron/pion discrimination. The lead-fiber assembly was basically the same as that used for the JETSET calorimeter at LEAR[1,2], differing principally in the longer length of the new modules.

## I Introduction

The CEBAF Large Acceptance Spectrometer (CLAS) detector [3] will consist of a superconducting toroidal magnet made of six coils, which are symmetrically arranged to form six identical sectors. Each sector will be equipped with drift chambers for charged particle tracking, scintillation counters for triggering and TOF measurements, gas Cerenkov counters and electromagnetic calorimeters for photon, electron, and pion identification and energy determination. Particular emphasis is put on electron and negative pion identification over a momentum range of 0.5 GeV/c to 4 GeV/c. The calorimeter prototype which is described here can serve as constituent elements for either the forward or barrel sections of the calorimeter.

Four modules were built, each with an effective radiation length (r.l.) of 1.63 cm. Two were to serve as Front blocks (9.8 cm depth, or 6 r.l.), and two as Back blocks (14.7 cm depth, or 9 r.l.)[4]. Each presents to incident particles an X by Y column profile of 120 cm by 9.2 cm. Phototube readout of light from the fibers is accomplished at both

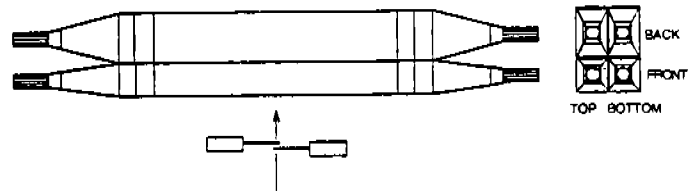


Figure 1: Detector setup in the beamline

polished ends via tapered, reflective aluminum air light guides. The phototubes view an epoxied matrix of 1 mm dia. scintillating fibers (Bicron BC-10) and 0.546mm thick lead (plus 6% Sb) plates which are grooved on both sides to offset fibers in adjacent rows by half a fiber spacing. By volume, material is distributed in a ratio of Fiber:Lead:Epoxy = 50:35:15.

In addition to measurements of the electron energy resolution and linearity for the overall calorimeter, event readout at both ends of modules allowed studies to be made of photoelectron statistics, position resolution of hits along the fiber axis X, and multiple measurements of signal attenuation in X. With one Front-Back pair of blocks mounted atop the other, studies could also be made of both longitudinal sampling differences for electrons and pions, and signal variations across the interface between module pairs.

## II Test Configuration

The A2 line at the Brookhaven National Laboratory

\*Supported by the U.S. Dept. of Energy and the National Science Foundation

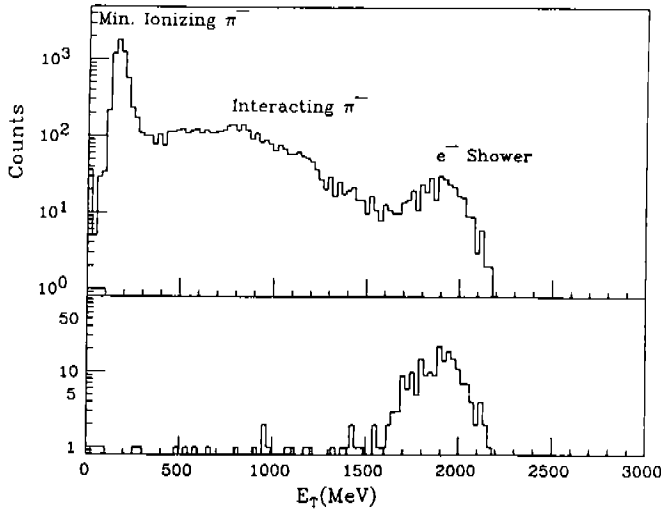


Figure 2: Response of the detector to pions and electrons

AGS facility provided a secondary beam composed primarily of pions, with a small component of electrons. With the exception of an energy measurement at 4 GeV, all other measurements were made at an energy of 2 GeV. Figure 1 shows both a top and side view of the two pairs of modules which were mounted upon an elevating table to facilitate changes in the X, Y entry point of the beam. The eight phototubes viewing the calorimeter were XP2262s mounted on CERN bases. Light guides were formed from sheets of 25 mil thickness ALCOA EverBrite which in turn coupled to the phototubes via Lucite cylinders of 4.45cm dia. Black masking tape was used to wrap individual modules, and to connect light guides to detector blocks.

Pions were selected in a three-fold coincidence between small plastic scintillators. The final two overlapped to define a beam spot of 1.3 by 1.9cm, 40cm upstream of the calorimeter. An electron tag was provided by two beam-line gas Cerenkov counters. Readout was accomplished with a LeCroy FERA system, which provided channels of ADC (Model 4300B) and TDC (Model 4300B and 4303) for each calorimeter phototube.

A beam tuned for a momentum of 2 GeV/c was injected, first into the center of the bottom pair of modules, followed by the top pair. High voltage was adjusted to balance separately the pedestal-adjusted, ADC spectra of minimum ionizing pions in the Front and Back block PMTs, and a calibration applied based on the expected mean energy loss. Figure 2 shows a resulting sum energy spectrum for the eight calorimeter channels both with and without the Cerenkov tag. For this case, trigger counters S2 and S3 were put in full overlap (4.1cm by 3.8cm) and the center of this beam entered 1cm below the midpoint of the top pair of modules.

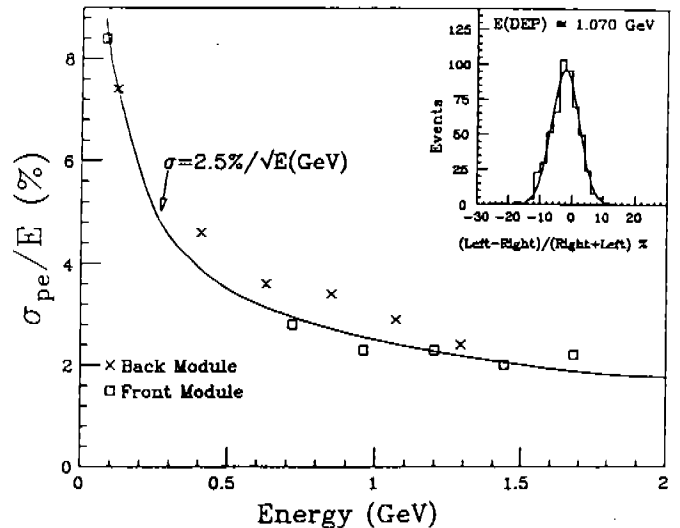


Figure 3: Contributions of photo-electron fluctuations to energy resolution

### III Detector Performance

#### III-A Photoelectron Statistics

The energy resolution  $\sigma_E$  of a sampling electromagnetic calorimeter is mainly given in quadrature by a combination of the following factors depending upon the beam energy and the detector geometry: 1) sampling fluctuations  $\sigma_s$ , which are variations for repeated events in the fraction of the deposited energy that is converted to a signal in the active part of the detector, 2) leakage fluctuations  $\sigma_l$ , which are changes in the fraction of a given energy contained by a detector, 3) photoelectron fluctuations  $\sigma_{pe}$ , which are variations in the number of photoelectrons released at the photocathode for otherwise repeated events, and 4) fluctuation in the light transmission through the detector to the photo multiplier tubes.

Since events in our modules were viewed by two phototubes, it was possible to extract a direct measurement of  $\sigma_{pe}$  behaviour for the PMT pair by forming a series of histograms of the difference in Left(L)/Right(R) pulse heights divided by the sum of pulse heights. Figure 3 presents the results of this study for the two bottom modules, showing the way the measured ratio  $\sigma_{pe}/E$  varies as a function of the deposited energy  $E$ . As indicated by the insert in Fig.3, events in a given histogram were characterized by the amount of energy deposited in a module. Pion spectra corresponding to a 2 GeV/c beam incident at  $X=0$  were used for this measurement. The variation in  $\sigma_{pe}$  is reasonably well parameterized by the statistical expression

$$\sigma_{pe}/E = 2.5\%/\sqrt{E} \quad (1)$$

From this, the number of photoelectrons per GeV of energy deposited in the detector can be calculated directly as

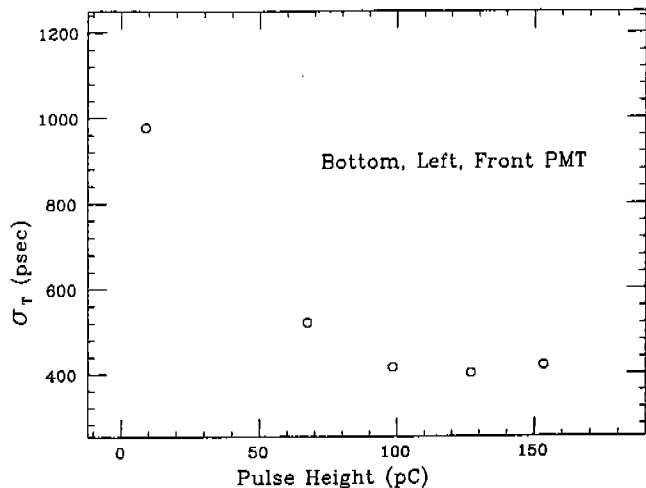


Figure 4: Timing resolution

$$N_{pe} = \frac{1}{\sigma_{pe}^2} \frac{\delta}{\delta - 1} = 2400(\text{GeV})^{-1} \quad (2)$$

where  $\delta$  is the amplification per dynode. As expected,  $\sigma_{pe}$  contributes negligibly to the energy resolution compared to sampling fluctuations.

### III-B Energy Resolution and Linearity

A Gaussian fit to the 2 GeV/c electron data in Fig.2b, in which the ADCs of the four modules were summed, yielded  $8.5\%/\sqrt{E}$ ; a similar fit for data taken at a momentum of 4 GeV/c gave  $10.5\%/\sqrt{E}$ . In as much as these blocks are enlarged versions of the ones described in Ref.[2], it had been expected that our resolution would better match the performance figure of  $6.3\%/\sqrt{E}$  established by Hertzog et al. This discrepancy has tentatively been traced to a nonuniform response of the different light guides. Both in a vertical beam scan taken for pions, and in a later study of these light guides using a scanning scintillating fiber, it was found that response increased by about 5% in the perimeter region of the light guide face.

A simple test for electron energy linearity was made by plotting fitted energies for the combined four module output against the expected beam energies of 2, and 4 GeV. A quadratic fit involving the origin and these two points is about one percent nonlinear.

### III-C Timing and Position Resolution

Given the large size of the blocks used here, and our hope to make others that are considerably larger, it is important to establish a figure for the position resolution of an event as calculated from the TDC information of the end phototubes. A plot of basic Gaussian timing resolution  $\sigma_t$  as a function of pulse height interval for an individual

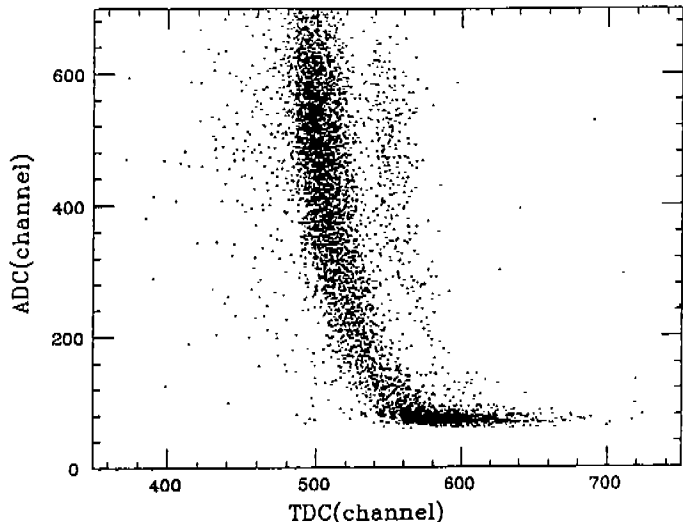


Figure 5: Pulse height vs time

phototube can characterize the timing performance. This is carried out in Figure 4 for the Bottom, Left, Front PMT, showing a range for  $\sigma_t$  from 970 psec at minimum ionizing pion pulse heights to 420 psec for electron signals.

The analysis for position resolution began with a necessary correction for TDC events which demonstrated a clear dependence on pulse height. This effect is evident in Figure 5 which shows a scatter plot of ADC vs. TDC data for a run at 2 GeV/c. A distinction can be made between electron events at large pulse heights and early times, and pion events at the lowest pulse heights and later times. This data was fit to an exponential function to parameterize the relationship between timing and pulse height. Based on this result, a correction was made to the TDC data which rendered the average TDC values constant over the full ADC range.

If a hit occurs at a distance  $X$  to the right of the detector center, then  $X$  can simply be related to the distance of the hit from the right PMT,  $S_r$ , and the distance from the left PMT,  $S_l$ , as

$$X = (S_l - S_r)/2 \quad (3)$$

Values for  $S_r$  and  $S_l$  were then calculated, using the corrected TDC times  $T_r$  and  $T_l$ , and the average speed of light in the scintillating fiber,  $v$ . This gives a working expression

$$X = v(T_l - T_r)/2 \quad (4)$$

for which the value of  $v$  was taken from a calibrating run of known distances  $S_r$  and  $S_l$ . Figure 6 shows the position resolution  $\sigma_x$  for the bottom two modules as a function of energy, with the beam incident at the nominal  $X=0$  position. This result was obtained by first forming Eq.4 histograms for data restricted to narrow energy intervals, as illustrated in the insert of Fig.6, and then fitting these distributions to a Gaussian function of width  $\sigma_x$ . The

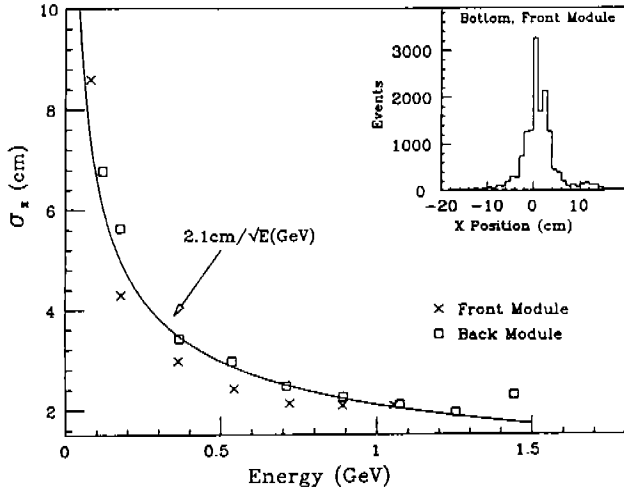


Figure 6: Position resolution vs energy

MODULE	PARTICLE	$\lambda$ (cm)
Bottom,Front	Pion	264
Bottom,Front	Electron	390
Bottom,Back	Pion	164
Bottom,Back	Electron	218

dependence of  $\sigma_x$  on energies less than 1.5 GeV is well parametrized by the expression

$$\sigma_x = 2.1(\text{cm})/\sqrt{E(\text{GeV})} \quad (5)$$

### III-D Attenuation Measurements

A study was carried out for the bottom blocks of the PMT signal attenuation vs the distance of the injected beam from each phototube. Limits on the X travel of the elevating table resulted in  $S_l$  values starting at 5 cm, followed by measurements in 10 cm steps from 10 to 80 cm. This same scan recorded data for the right phototube over the corresponding range of  $S_r = 115\text{cm}$ , followed by readings in 10 cm steps from 110 to 40 cm. Since two data points are given with each event, we decided to combine the attenuation information of both phototubes, first normalizing the left and right signals at  $S_l = S_r = 60\text{cm}$ , i.e.,  $X=0$ . At each position, separate pion and electron runs were taken. Figure 7, which shows the scan of the bottom, front module for 2 GeV electrons, gives evidence for both a short  $\lambda_1$  and a long  $\lambda_2$  attenuation length component. Table I shows the complete attenuation results for electron and pions in both bottom blocks, where a single exponential was fit to data points for  $S = 40\text{cm}$  and longer.

These results, overall, suggest longer  $\lambda$  values for electrons, compared to minimum ionizing pions. This behaviour, as well as the lack of agreement for the two mod-

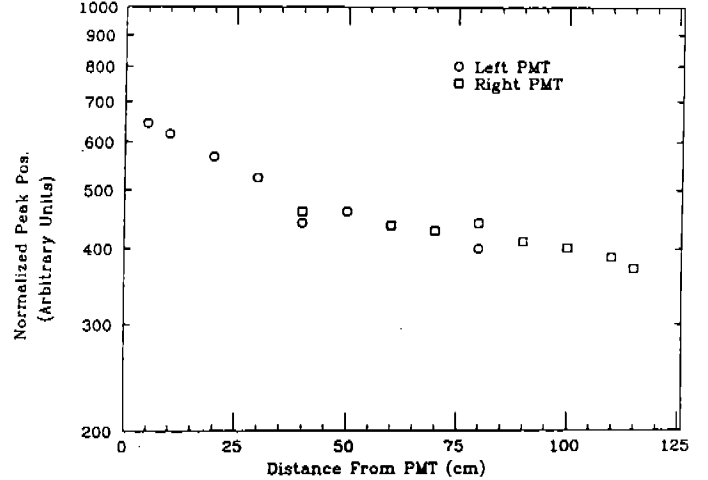


Figure 7: Calorimeter response vs horizontal position

ules, is not understood at this point.

### III-E Pion-Electron Discrimination

From the segmentation into a front and back part we expect a very good pion rejection capability. At 2 GeV, a preliminary analysis that makes use of the total energy deposition only gives a pion rejection of more than 98.5% at an electron detection efficiency of greater than 98%. From a more complete analysis that takes into account the full energy deposition pattern, as well as the transverse shower distribution, we expect this figure to improve even further.

## IV Conclusions

We have built and tested a lead/scintillating fiber calorimeter prototype with left-right readout. It measures electron shower energies with a resolution of  $9\%/\sqrt{E(\text{GeV})}$ , and allows a measurement of the shower position along the fiber axis to  $2.1\text{cm}/\sqrt{E(\text{GeV})}$ . Its time resolution for electron showers of 2 GeV is better than 0.5 nsec, and it can be used to reject more than 98.5% of 2 GeV pions, if the pion momentum is known. We are continuing tests to better understand its light attenuation properties.

## V Acknowledgements

We would like to thank the Brookhaven National Laboratory for making the AGS test beam available to us. We are indebted to D. Dayton of BNL who was an invaluable source of support. We wish to thank A. Carroll, D. Loewenstein, and P. Pile for their support during the heavy ion running.

## VI References

1. JETSET: Physics at LEAR with an Internal Gas Jet Target and an Advanced General Purpose Detector, Experiment PS202, CERN/PSCC 86-23, CERN, Freiburg, Genoa, Illinois, Julich KFA, Oslo, Upsala.
2. A High-Resolution Lead/Scintillating Fiber Electromagnetic Calorimeter, IULL-(NPL)-90-001, D.W. Hertzog et al.
3. Conceptual Design Report, CEBAF/SURA, April, 1990.
4. These modules were fabricated at the Nuclear Physics Laboratory of the University of Illinois in the same manner and with the same material as described in Ref.[2].